RSC Advances

PAPER

Published on 01 September 2026
Licensed under CC-BY-NC 4.0

Check for updates

Cite this: *RSC Adv.*, 2026, **16**, 51338

Plasmon-enhanced nonlinear optical response in Au–SnS_2 nanohybrids for optical limiting applications

Adarsh Raj K. P.,[a] Hasana Jahan Elamkulavan,[a] Anoop C. Sathyadevan Nair,[a] Abhinand Ramachandran,[bc] Abhijith Thazhathenair,*[bc] Chandrasekharan Keloth*[a] and Vari Sivaji Reddy*[a]

Integrating plasmonic metal nanoparticles (NPs) with semiconductor nanostructures is widely used as an invaluable tool for tailoring the light–matter interaction and thereby improving the nonlinear optical activity of the latter. In the present work, inherent plasmonic effects of spherical Au NPs of size 20 nm were utilized to enhance the nonlinear optical absorption of SnS_2 nanoplates of lateral size 890 nm. The pristine SnS_2 nanoplates exhibited significant reverse saturable absorption with an effective nonlinear absorption coefficient (β_{eff}) of 50 cm GW^{-1}, which increased to 85 cm GW^{-1} after incorporation of Au NPs, when their nonlinear optical characteristics were investigated using an open-aperture Z-scan technique with a nanosecond pulsed laser operating at a wavelength of 532 nm. The enhancement in nonlinear optical absorption is mainly attributed to the strong influence of plasmonic *hotspots* of Au NPs, whose characteristic resonance range (450–600 nm) aligns with the laser wavelength. The interaction of such intense plasmonic fields with SnS_2 nanoplates was further confirmed by simulating *E*-field intensity enhancement profiles using the finite-difference time-domain (FDTD) method. Furthermore, Au–SnS_2 nanohybrids exhibited excellent optical limiting behavior with an onset value of 0.07 J cm^{-2} and a low limiting threshold of 1.16 J cm^{-2}, which are found to be very significant compared to the values previously reported for eminent 2D materials and their nanohybrids. These findings highlight the significance of the present strategy in developing nanohybrids to enhance the nonlinear optical activity of conventional semiconductor nanosystems.

Received 13th June 2026
Accepted 21st August 2026

DOI: 10.1039/d6ra05188j

rsc.li/rsc-advances

Introduction

Nanotechnology offers a viable route to overcome the limitations of individual semiconductor materials in controlling the inherent photophysical processes, including excitonic dynamics, free-charge-carrier generation, and their transport.[1,2] Engineering the dimensionality of bulk semiconductors to the nanoscale induces new electronic, optical, and mechanical properties and thereby establishes a versatile platform to achieve enhanced tunability of these conventional characteristics.[1] Owing to such superior characteristics attained *via* nanoscaling, the two-dimensional materials such as graphene, metal dichalcogenides (MDCs), and MXenes have been extensively explored for modern electronics, optoelectronics, energy storage and conversion, sensing technologies, and photonics.[3,4]

Due to the rapid growth in the use of high-power lasers in areas such as optical communication systems, industrial machining, military gadgets, and biomedical devices, there is an increasing demand for the development of high-performance laser safety materials. In this context, the 2D materials exhibiting third-order nonlinear absorption with high optical limiting activity are particularly suitable for the development of laser safety devices.[5]

The MDCs, an emerging class of 2D materials, exhibit variety of nonlinear optical (NLO) phenomena such as saturable absorption, reverse saturable absorption, second and third harmonic generation making them suitable for various interesting applications including frequency conversion, mode-locking, Q-switching, and optical limiting.[6–8] The superior optical nonlinearity of MDCs arises from the layer dependent band gap, and strong excitonic effects.[5,8] The chemical structure of MDCs is denoted as MX_2, where M represents a metal atom (Mo, W, Nb, Sn, V, *etc.*) and X represents a chalcogenide atom (S, Se and Te). Here, the metal atom is sandwiched between two layers of chalcogenide atoms. Within these materials, the surface chalcogenide atoms exhibit no dangling bonds and are

[a]*Department of Physics, National Institute of Technology Calicut (NITC), Kerala-673601, India. E-mail: sivaji@nitc.ac.in; csk@nitc.ac.in*

[b]*Department of Physics, PSG Institute of Technology and Applied Research, Neelambur, Coimbatore, Tamil Nadu-641062, India. E-mail: abt@psgias.ac.in*

[c]*Department of Nanoscience and Technology, PSG Institute of Advanced Studies, Peelamedu, Coimbatore, Tamil Nadu-641004, India*

© 2026 The Author(s). Published by the Royal Society of Chemistry

covalently bonded to the central metal atoms, resulting in excellent chemical stability.[9]

Among MDCs, SnS_2 has been widely explored for diverse applications including solar cells,[10] transistors,[11] photodetectors,[12] photocatalysis[13] and sensors[14] due to its superior optoelectronic properties, direct wide bandgap and environment friendly nature.[10–15] The nonlinear optical properties such as reverse saturable absorption (RSA) and saturable absorption (SA) have been reported in the nanostructures of SnS_2.[16,17] Various methods like doping, defect engineering and hybrid formation were effectively used to enhance the NLO response of SnS_2 nanostructures.[17–20] Wu *et al.* reported nonlinear optical absorption in hydrothermally synthesized SnS_2 nanosheets using the Z scan technique with nanosecond and picosecond laser pulses.[16] An optical limiting threshold of 0.23 J cm^{-2} was obtained using 532 nm picosecond laser. Diao *et al.* achieved a nine-fold enhancement in nonlinear absorption coefficient in hydrothermally synthesized SnS_2 nanosheets using Ar plasma treatment.[18] Formation of in-gap states due to creation of sulfur vacancies during plasma treatment, which act as intermediate states that induce excited state absorption (ESA) during femtosecond laser excitation, was found to be responsible for the large improvement in nonlinear optical response. Wei *et al.* demonstrated covalent functionalization of SnS_2 with porphyrin as an effective method for achieving ultrafast optical limiting.[17] Ke *et al.* achieved enhancement in saturable absorption, two-photon absorption and three-photon absorption under femtosecond laser excitation across a broad wavelength range (515–1550 nm) using electrostatic doping of SnS_2 *via* proton intercalation for optical neural network applications.[19] Li *et al.* constructed a SnS_2/cetyltrimethylammonium superlattice and obtained significant nonlinear absorption enhancement across a broad wavelength range due to dielectric confinement and bandgap reduction effects.[20]

Plasmonic effects of metal nanostructures are widely utilized in solar cells,[21] photodetectors,[22] photocatalysis[23] and SERS applications[24] to boost light–matter interaction. The localized surface plasmon resonance (LSPR) arising from the collective oscillation of surface electrons in metal nanostructures enhances electromagnetic fields around the metal nanostructures.[25] Especially, when metal nanostructures of size below 20 nm are incorporated in a medium, large electromagnetic fields generated around the nanostructures can significantly improve the optical properties of the surrounding medium.[26] In some recent studies, the LSPR effects of metal nanostructures have been effectively used to improve the NLO properties of MDCs like MoS_2 and WS_2.[27,28] Significant improvement in photochemical sensing, photodetection and photocatalytic activities of SnS_2 nanostructures has been achieved by utilizing LSPR effects of Au nanostructures such as near-field enhancement and hot-electron injection.[29–31] Though both these effects are useful for improving light–matter interaction, to the best of our knowledge, these effects are not utilized for enhancing NLO response of SnS_2 nanostructures.

In the present study, plasmonic effects of Au NPs were successfully employed to improve the nonlinear optical absorption of SnS_2 nanoplates. The size of chemically synthesized Au NPs was strategically tuned such that the laser wavelength lies perfectly within the plasmonic band of Au NPs to induce resonant absorption. The Raman spectroscopy and finite-difference time-domain (FDTD) simulations were employed to understand the role of Au NPs in improving the nonlinear optical response of SnS_2 nanoplates. The simulation results revealed the generation of intense electric field around Au nanoparticles. The interaction of this plasmonic field with the SnS_2 nanoplates resulted in improved nonlinear absorption leading to enhanced optical limiting properties. Through the correlation between experimental observations and simulation results, a mechanism was proposed to elucidate plasmon resonance enhanced nonlinear optical response in Au–SnS_2 nanohybrids.

Experimental procedure

For the synthesis of Au–SnS_2 nanohybrids, chemicals such as tin chloride pentahydrate ($SnCl_4 \cdot 5H_2O$) (98%, Sigma-Aldrich), thiourea (CH_4N_2S) (99%, Sigma-Aldrich), gold(III) chloride hydrate ($HAuCl_4 \cdot xH_2O$) (99.995%, Sigma-Aldrich), and trisodium citrate ($HOC(COONa)(CH_2COONa)_2 \cdot 2H_2O$) (99%, Merck) were purchased and used without any further purification. The SnS_2 nanostructures were synthesized through a one-step hydrothermal process as schematically represented in Fig. 1(a).[32] In this procedure, 2 mmol of tin chloride pentahydrate and 8 mmol of thiourea were mixed in 20 ml of DI water and stirred for 30 min until the solution becomes clear. The solution was then moved to a 100 ml autoclave reactor and maintained at 180 °C for 12 h in a hot air oven. Subsequently, the system was allowed to cool naturally and the yellow colour precipitate was collected by centrifugation. Here, an excess amount of thiourea was used to provide sulfur-rich environment which facilitates the controlled nucleation and growth of SnS_2 nanoplates. The precipitate was washed several times with deionized water and ethanol to remove the unreacted precursors and impurities, followed by drying in vacuum at 60 °C for 6 h.

For the preparation of Au–SnS_2 nanohybrid, Au nanoparticles were separately synthesized by citrate reduction method.[33] In this method, gold(III) chloride hydrate ($HAuCl_4 \cdot xH_2O$) was used as the Au precursor and trisodium citrate acted as both reducing and stabilising agent. Initially, 10 ml of 0.5 mM aqueous gold chloride was boiled using a magnetic stirrer-hot plate arrangement. Then, 0.5 ml of 38.8 mM trisodium citrate solution was injected into the boiling aqueous gold chloride solution. The colourless solution slowly changed to faint blue and then to red wine colour after 15 min of boiling indicating the formation of mono-dispersed Au nanoparticles. For the preparation of Au–SnS_2 nanohybrids, the synthesized Au nanoparticles were directly used, without any further purification. The nanohybrids were prepared by adding 0.75 ml of Au NP solution (0.17 mg ml^{-1}) to 1 ml dispersion of SnS_2 nanoplates (0.5 mg ml^{-1}), followed by continuous overnight stirring to ensure uniform mixing of the nanostructures. No additional purification was performed to remove Au nanoparticles that remained unattached to the SnS_2 surface. The morphology of

© 2026 The Author(s). Published by the Royal Society of Chemistry

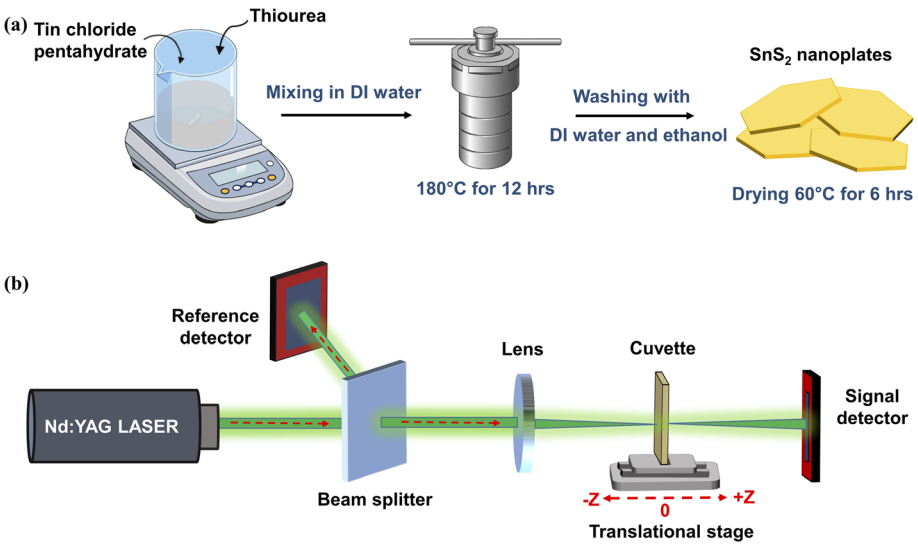


Fig. 1 Schematic diagrams showing (a) synthesis of SnS_2 nanoplates and (b) open aperture Z-scan experimental setup.

the nanostructures was analysed using a high-resolution transmission electron microscopy (HR-TEM) (JEOL JEM 2100) and field emission scanning electron microscopy (FE-SEM) (ZIESS, Gemini 1, Sigma 300). The formation and phase purity of SnS_2 nanostructures were confirmed using an X-ray diffractometer (XRD) with Cu K_α radiation (Rigaku smart lab SE). The colloidal stability of the nanostructures was studied using the Zeta potential measurement (Microtrac, PMX 500). The linear absorption of the nanostructures was recorded using an UV-visible spectrophotometer (PerkinElmer Lambda 365+). For this study, the Au nanoparticle and SnS_2 nanoplate solutions were prepared with concentrations 0.017 mg ml^{-1} and 0.029 mg ml^{-1}, respectively, by suitably diluting initial solutions with DI water. In the case of Au–SnS_2 nanohybrid, 1 ml solution contained 0.029 mg of SnS_2 nanoplates and 0.0073 mg of Au nanoparticles. The electric field intensity distribution around the Au NPs was simulated using a commercially available Ansys Lumerical FDTD simulation software.

To investigate the NLO properties of SnS_2 nanoplates, open aperture Z-scan measurements were carried out with a Q-switched Nd:YAG pulsed laser (Quanta Ray, Spectra Physics) operating at 532 nm wavelength with a 7 ns pulse width and 10 Hz repetition rate. Fig. 1(b) shows the schematic diagram of Z-scan arrangement, where a convex lens of 15 cm focal length was used to focus the beam onto the sample. Before the measurement, sample was taken in a cuvette of thickness 1 mm and diluted using DI water to obtain 80% linear transmittance. The diluted Au nanoparticle and SnS_2 nanoplate solutions have concentrations of 0.17 mg ml^{-1} and 0.05 mg ml^{-1}, respectively. On other hand, 1 ml of nanohybrid contained 0.0435 mg of SnS_2 nanoplates and 0.011 mg of Au nanoparticles. Then the sample was fixed at the focal plane where the beam waist and Rayleigh range were 17.5 μm and 1.8 mm, respectively. The nonlinear scattering was found negligible when measured using a detector positioned at 45° from the sample. The Z-scan measurements were performed at two pulse energies, 10 μJ and 20 μJ, corresponding to peak on-axis intensities of 0.27 GW cm^{-2} and 0.55 GW cm^{-2}, respectively. The incident pulse fluence was varied by adjusting the output pulse energy of the laser while maintaining identical experimental conditions. The pulse energy corresponding to each measurement was monitored using a calibrated laser energy meter to ensure accurate determination of the incident fluence. The Raman spectra of the SnS_2 nanoplates and Au–SnS_2 nanohybrid were recorded using a HORIBRA, LabRam HR Evo confocal Raman spectrometer operating at a 532 nm excitation wavelength and 5 mW excitation power. The concentrations of solutions used for the measurement of Raman spectra are same as those used for Z-scan measurements.

Results and discussion

The morphology of hydrothermally synthesized SnS_2 nanostructures was studied using FE-SEM and HR-TEM. The FE-SEM image shown in Fig. 2(a) and the size distribution histogram presented in Fig. S1 reveal the formation of hexagonal SnS_2 nanoplates with an average size of 890 nm. Further, the approximate thickness of the nanoplates was found to be around 70 nm as shown in Fig. S2. The EDS spectrum shown in Fig. S3 reveals the presence of Sn and S in the nanostructures with a ratio of 1 : 1.54. The EDS colour mapping images presented in Fig. S4 confirm the uniform distribution of Sn and S in the sample. The hexagonal SnS_2 nanoplates with sharp edges were also observed in the HR-TEM image shown in Fig. 2(b). The lattice fringes with a spacing of 0.32 nm shown in the inset of Fig. 2(b) correspond to (100) planes of hexagonal SnS_2.[34] The SAED pattern recorded on a single SnS_2 nanoplate contains an ordered array of sharp spots confirming the single crystalline nature of the SnS_2 nanoplates (Fig. 2(c)). From the SAED pattern, *d*-spacing values of 0.32 nm and 0.18 nm were obtained which match well with the (100) and (110) planes of hexagonal phase of SnS_2.[34] The crystal structure of SnS_2 nanoplates was further analysed using XRD measurements. The XRD pattern shown in Fig. S5 contains peaks at 15.02°, 28.23°, 32.12°, 41.89,

© 2026 The Author(s). Published by the Royal Society of Chemistry

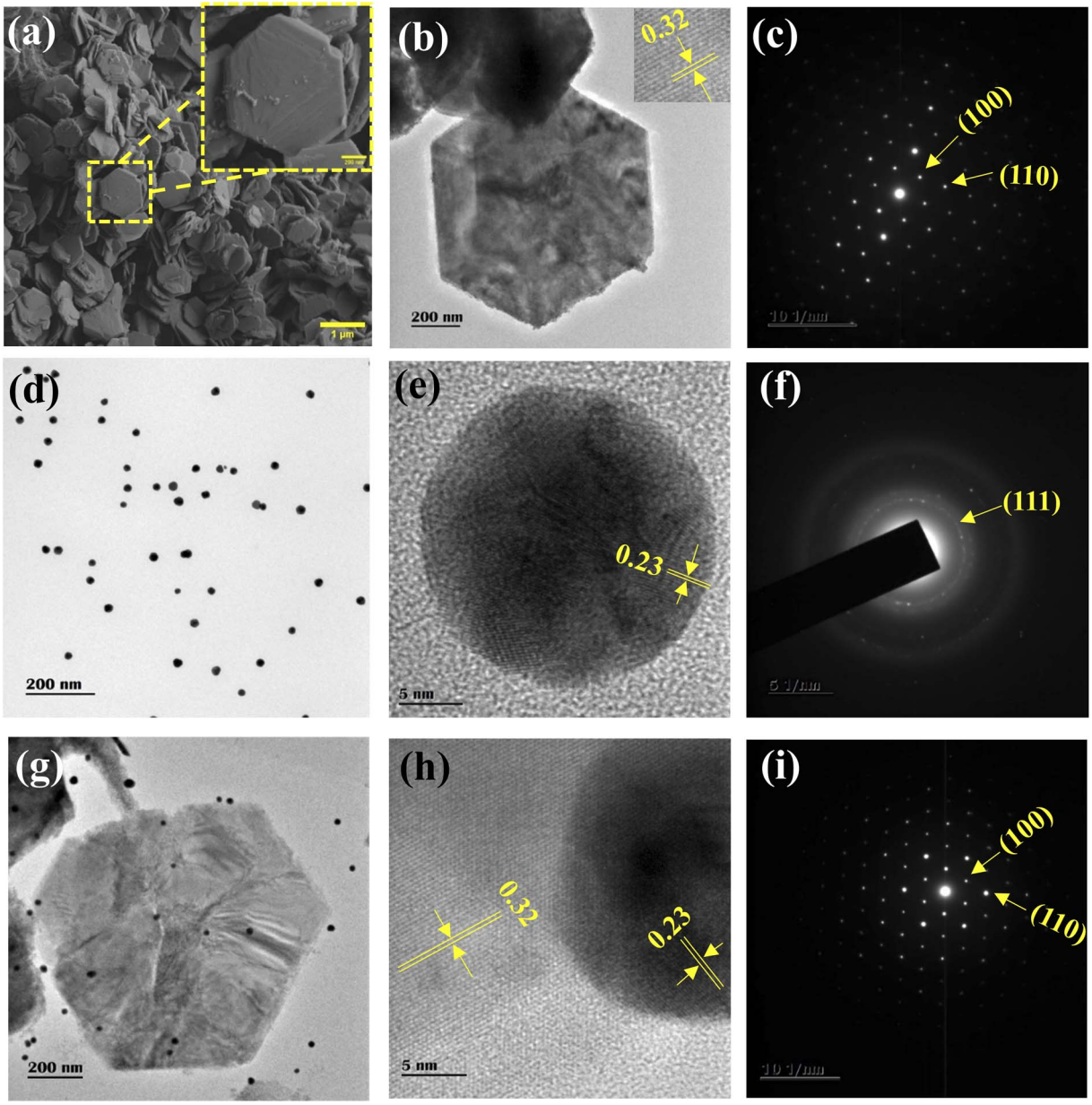


Fig. 2 (a) FE-SEM image, (b) HR-TEM image (inset: magnified image showing lattice fringes), and (c) SAED pattern of SnS_2 nanoplates. (d) HR-TEM image, (e) magnified TEM image with lattice fringes and (f) SAED pattern of Au nanostructures. (g) HR-TEM image, (h) magnified HR-TEM image with lattice fringes and (i) SAED pattern of Au–SnS_2 nanohybrid.

46.12°, 59.96°, 52.41°, 55.17°, 60.66° and 67.37° corresponding to the hexagonal crystal structure of SnS_2 (JCPDS No. 023-0677).[35] In addition, the absence of any impurity peaks in the XRD pattern confirms the formation of high purity SnS_2 nanostructures.

The Au nanoparticles were synthesized using citrate reduction method as it offers excellent control over the size and shape of nanostructures compared to other methods like pulsed laser ablation.[36] The HR-TEM image of synthesized Au NPs is shown in Fig. 2(d). Highly uniform spherical nanoparticles with an average diameter of 20 nm were observed as shown in the size distribution histogram presented in Fig. S6. Presence of lattice fringes with a *d*-spacing value of 0.23 nm was observed in the magnified HR-TEM image shown in Fig. 2(e) which correspond to (111) planes of fcc gold.[37] Concentric rings observed in the SAED pattern presented in Fig. 2(f) indicate that the synthesized Au nanoparticles are polycrystalline. The HR-TEM image of Au–SnS_2 nanohybrid shown in Fig. 2(g) and S7 reveals the uniform distribution of Au nanoparticles on the surface of SnS_2 nanoplates. The lattice fringes corresponding to both Au and SnS_2 were observed in the magnified HR-TEM image of Au–SnS_2 nanohybrid shown in Fig. 2(h). On the other hand, the SAED pattern of nanohybrid mainly contained a systematic array of spots corresponding to SnS_2 nanoplates due to the low concentration of Au NPs (Fig. 2(i)).

© 2026 The Author(s). Published by the Royal Society of Chemistry

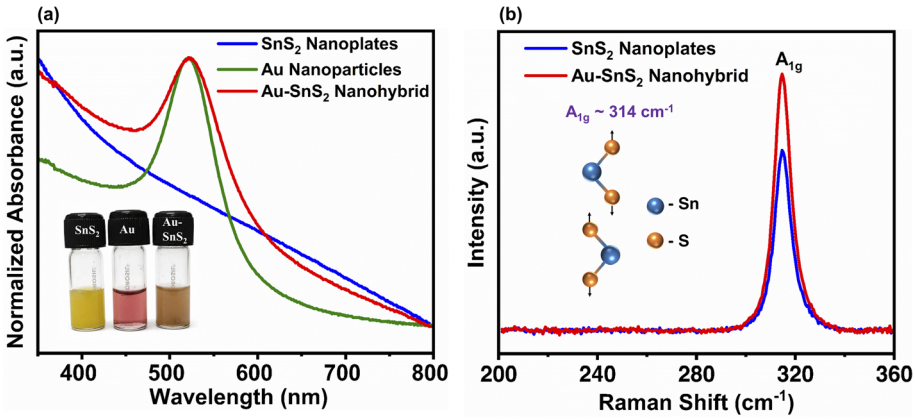


Fig. 3 (a) UV-visible absorption spectra of SnS_2 nanoplates, Au NPs and Au–SnS_2 nanohybrid. (b) Raman spectra of SnS_2 nanoplates and Au–SnS_2 nanohybrid.

The linear optical properties of Au NPs, SnS_2 nanoplates and Au–SnS_2 nanohybrid were studied by measuring UV-vis absorption spectra and are presented in Fig. 3(a). The SnS_2 nanoplates exhibited a broad absorption in the visible range which increased sharply below 500 nm. A band gap energy of 2.23 eV was obtained for SnS_2 nanoplate sample using Tauc plot method as shown in Fig. S8 which is in agreement with earlier reports.[38] On the other hand, Au NPs showed a distinct plasmonic band in the wavelength range 450–600 nm with a peak at 521 nm. This strong absorption peak arises from the collective oscillation of conduction electrons on the surface of Au NPs during the excitation of light. The absorption spectrum of Au–SnS_2 nanohybrid contained the combined characteristics of both the Au NPs and SnS_2 nanoplates. In spite of the lower amount of Au NPs in the Au–SnS_2 nanohybrid, the absorption spectrum contained a clear plasmonic band which is beneficial for improving the nonlinear optical properties of SnS_2 nanoplates.

To further understand the surface plasmon resonance effect of Au NPs, Raman spectra of the samples were recorded and presented in Fig. 3(b). The Raman spectra of both pristine SnS_2 and Au–SnS_2 nanohybrid contained a sharp peak at 314 cm^{-1} that corresponds to A_{1g} mode representing out of plane vibration of S atoms in opposite directions with respect to Sn atom.[35] The Au–SnS_2 nanohybrid exhibited significantly higher intensity compared to pure SnS_2 nanoplates, which is attributed to the LSPR effect of Au NPs distributed on the surface of SnS_2 nanoplates. However, no additional peaks or shifting of peaks were observed in both the absorption and Raman spectra of Au–SnS_2 nanohybrid indicating that there is no strong chemical interaction between the Au nanoparticles and the SnS_2 nanoplates. A weak van-der-Waals type physical interaction is expected between Au nanoparticles and the SnS_2 nanoplates.

Prior to nonlinear optical measurements, colloidal stability of the samples prepared in DI water was tested by measuring the zeta-potential values. The Au nanoparticles, SnS_2 nanoplates and the Au–SnS_2 nanohybrids exhibited average zeta-potential values of −70.5 mV, −50.2 mV and −66.4 mV, respectively. These values indicate high colloidal stability of all the samples which is essential for conducting optical measurements over a long period. Moreover, the Au–SnS_2 nanohybrid has shown high stability under laser light illumination and also with time as shown in Fig. S9. The nonlinear optical properties of pure nanostructures and the nanohybrid were investigated using open aperture Z-scan measurements with a Q-switched Nd:YAG laser operated at 532 nm excitation wavelength as schematically shown in Fig. 1(b). The NLO response of SnS_2 nanoplates, Au NPs and Au–SnS_2 nanohybrids at two different pulse energies 10 μJ and 20 μJ is presented in Fig. 4(a) and (b). At 10 μJ pulse energy, Au NPs did not exhibit any noticeable nonlinear response. Whereas, in the case of SnS_2 nanoplates and Au–SnS_2 nanohybrid a continuous decrease in the transmittance was noticed when the sample was moved closer to the focus with a minimum transmittance at the focus, indicating the presence of RSA-like behaviour. The minimum transmittance at 10 μJ pulse energy was found to be 0.60 and 0.49 for SnS_2 nanoplates and Au–SnS_2 nanohybrid, respectively.

To further understand the nonlinear absorption properties, the nonlinear optical parameters were calculated by fitting the experimentally obtained optical response with nonlinear propagation equation, which includes the SA and RSA activities

$$\frac{dI}{dz} = -\left(\frac{\alpha_0}{1+\frac{I}{I_{sat}}} + \beta_{eff} I\right) I \quad (1)$$

where α_0, β_{eff}, I, and I_{sat} denote the linear and nonlinear absorption coefficients, input intensity, and saturation intensity, respectively. In eqn (1), the first and the second terms denote the SA and RSA components, respectively. The parameters I_{sat} and β_{eff} represent the contribution of SA and RSA to the NLO response of the sample. Here, I_{sat} denotes the characteristic incident intensity at which saturation effects become significant, while β_{eff} describes the strength of the nonlinear absorption. The calculated NLO parameters of Au NPs, SnS_2 nanoplates and Au–SnS_2 nanohybrid at pulse energies 10 μJ and 20 μJ are summarized in Table 1. The uncertainty in the extracted nonlinear optical parameters was estimated to be within approximately 7%, based on the established experimental uncertainty of our open aperture Z-scan setup, as

© 2026 The Author(s). Published by the Royal Society of Chemistry

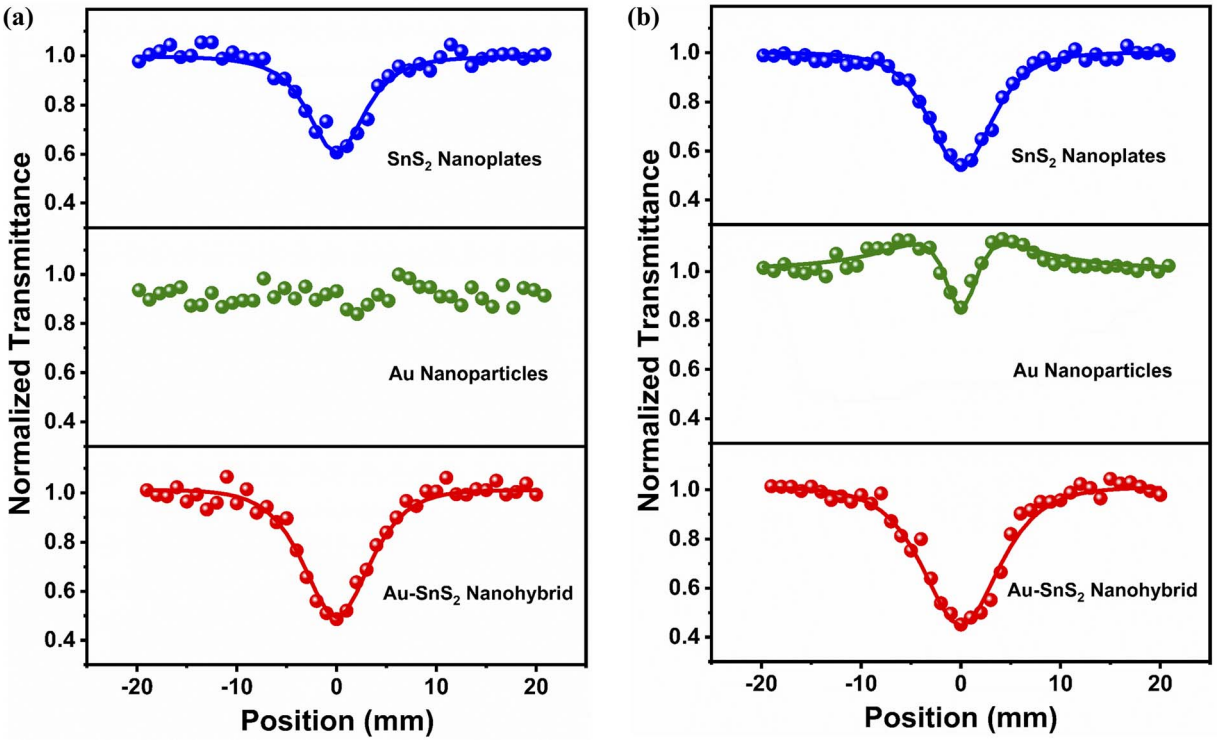


Fig. 4 Nonlinear optical response SnS_2, Au–SnS_2 and Au nanostructures at a pulse energy of (a) 10 μJ and (b) 20 μJ.

reported in our earlier work.[39] This uncertainty mainly arises from pulse-to-pulse laser energy fluctuations, beam alignment, detector response, and fitting uncertainties. The nonlinear absorption coefficient of pure SnS_2 nanoplate sample at 10 μJ pulse energy was found to be 50 cm GW^{-1}. Significant improvement in the nonlinear optical response of SnS_2 nanoplates was noticed after adding Au NPs leading to a high β_{eff} value of 85 cm GW^{-1}. Although Au NPs alone have not shown any considerable NLO response at 10 μJ energy, their incorporation into SnS_2 nanoplates resulted in 1.7 times enhancement in the value of β_{eff}. In addition, the Au–SnS_2 nanohybrid exhibited significantly lower I_{sat} values than the pristine SnS_2 nanoplates at both investigated pulse energies, indicating a lower characteristic saturation intensity. Together with the enhanced β_{eff}, these results indicate an improved nonlinear optical response upon Au incorporation.

The nonlinear optical response of the samples at 20 μJ pulse energy is shown in Fig. 4(b). Unlike at the 10 μJ energy, Au NPs exhibited a significant nonlinear absorption at 20 μJ energy, with two humps appearing on either side of the valley in Z-scan profile. This feature indicates an interplay of SA and RSA with SA dominating away from the focal point and RSA leading at the focal point. The SA response arises from the depletion of ground state population due to resonant absorption of Au nanoparticles which prevents further absorption leading to slight increase in transmittance.[40] Further increase in intensity resulted in sharp reduction in the transmittance value leading to RSA-like behavior. The β_{eff} value of pure Au NPs was found to be 9 cm GW^{-1} at 20 μJ pulse energy. While Au NPs exhibited improved nonlinear absorption at 20 μJ pulse energy, it is significantly weaker than that of bare SnS_2 nanoplates which showed a β_{eff} value of 37 cm GW^{-1}. On the other hand, the Au–SnS_2 nanohybrid showed an enhanced nonlinear activity with a β_{eff} of 56 cm GW^{-1}, which is 1.5 times higher than the bare SnS_2 nanoplates at 20 μJ pulse energy.

Enhancement in the intensity of SnS_2 Raman peak after incorporating Au NPs indicates that there is improvement in light–matter interaction due to the plasmonic effects of nanoparticles. To further understand the role of plasmonic effects in improving the nonlinear absorption, FDTD simulations were performed on Au–SnS_2 nanohybrid. The morphological characterization of Au–SnS_2 nanohybrid revealed the presence of isolated Au NPs of size 20 nm on the surface of hexagonal SnS_2 nanoplates. In addition, nanoparticles separated by smaller gaps were also observed in few locations. Therefore, to match with the experimental observations, a pair of 20 nm sized Au NPs separated by various possible distances in the range 1–20 nm were modelled. The Au NPs were placed on an SnS_2 nanoplate of thickness 70 nm kept on the $x - y$ plane as shown in Fig. 5(a). The simulation structure was illuminated using

Table 1 Calculated NLO parameters of Au NPs, SnS_2 nanoplates and Au–SnS_2 nanohybrid at two different pulse energies

Pulse energy	Nanostructure	I_{sat} (10^{-2} GW cm^{-2})	β_{eff} (cm GW^{-1})
10 μJ	Au	—	—
	SnS_2	4.49	50
	Au–SnS_2	1.49	85
20 μJ	Au	5	9
	SnS_2	6	37
	Au–SnS_2	2.8	56

© 2026 The Author(s). Published by the Royal Society of Chemistry

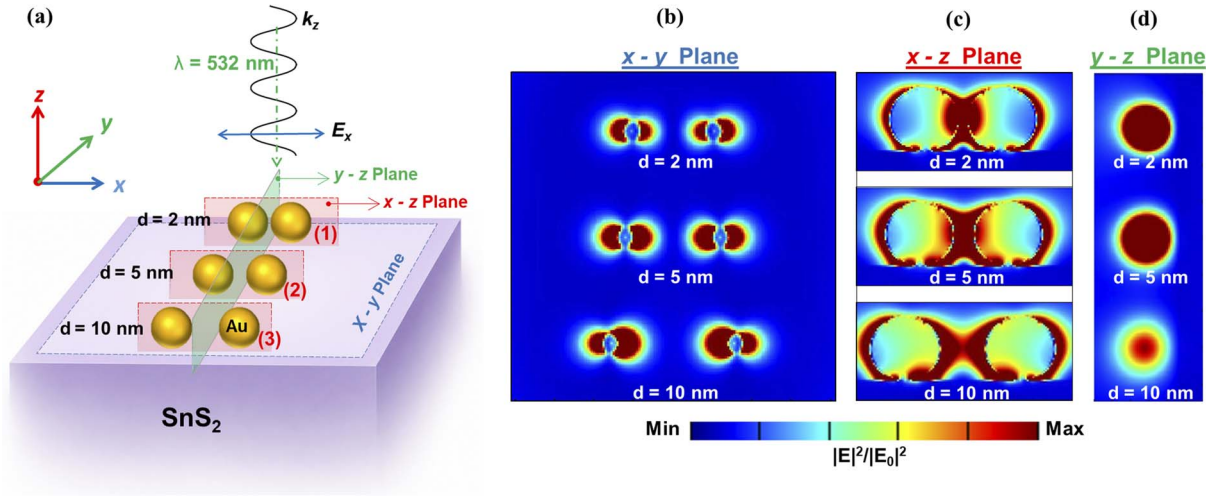


Fig. 5 (a) Schematic representation of FDTD simulation structure, and (b) electric field intensity enhancement on (b) $x-y$, (c) $x-z$ and (d) $y-z$ cross-sections for different inter-particle separations.

a total-field scattered-field (TFSF) light source with a wavelength of $\lambda = 532$ nm, *E*-field polarization along the *x*-axis (E_x), and propagation along the -*z* direction (k_z). The simulations were performed by taking the refractive index and extinction coefficient of SnS_2 at 532 nm wavelength as 2.97 and 0.029, respectively, as reported by Ermolaev *et al.*[41] The *E*-field intensity enhancement during illumination was monitored on $x-y, y-z$ and $x-z$ cross-sections using five frequency domain power monitors as indicated in Fig. 5(a). To attain high accuracy in simulation results, a mesh size of 0.5 nm was used in the simulation region. The simulations were performed by applying the perfectly matched layer (PML) boundary conditions along *z*-direction and symmetric boundary conditions in both *x*- and *y*-directions. The simulation results corresponding to the particle separations, $d = 2$, 5 and 10 nm are presented in Fig. 5(b–d). In the case of larger separations above 10 nm, very strong plasmonic field was observed on the $x-y$ and $x-z$ cross-sections as shown in Fig. 5(b) and (c). These profiles clearly indicate that the induced *E*-field is mainly concentrated on the lateral sides of the Au nanoparticles in the *x*-direction. On the other hand, the *E*-field was found to be relatively weaker on the $y-z$ cross-section since the incident light polarization is along *x* direction. When the particle separation was decreased below 5 nm, formation of *hotspots* (high *E*-field intensity regions) was noticed due to the coupling of plasmon oscillations in neighbouring nanoparticles. The presence of strong *E*-field was observed on all the three cross-sections $x-y$, $x-z$ and $y-z$ as shown in Fig. 5(b–d). Interaction of this intense plasmonic field with the SnS_2 nanoplates can significantly boost the light–matter interaction in Au–SnS_2 nanohybrid.

The nonlinear absorption phenomena in pristine SnS_2 nanoplates is schematically illustrated in Fig. 6(a). Here, S_0, S_1

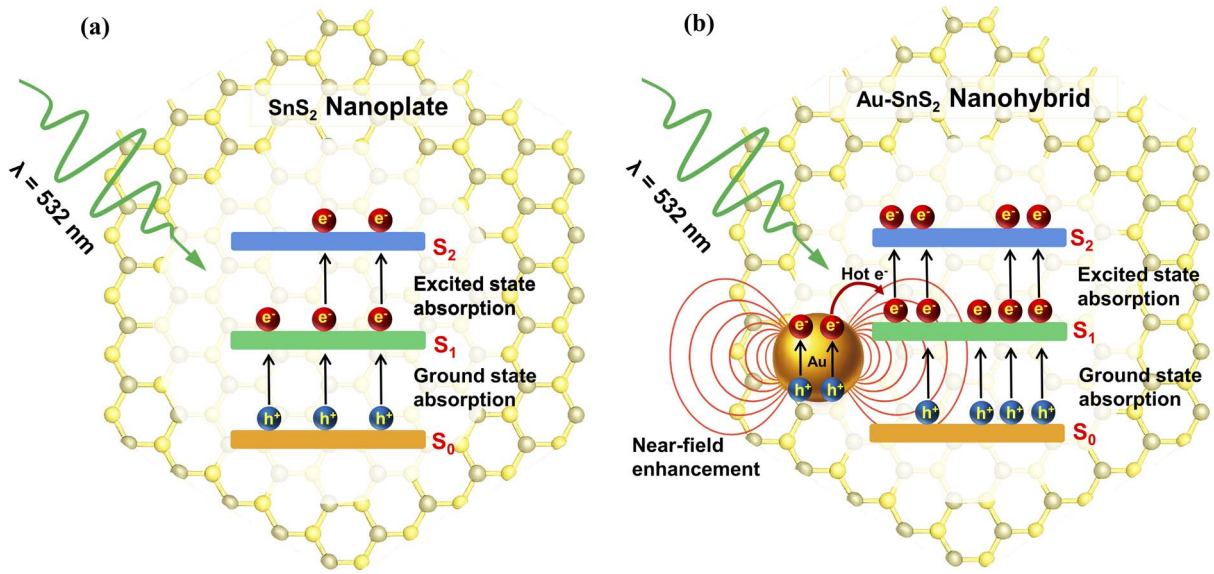


Fig. 6 Schematic illustration of nonlinear absorption phenomena in (a) pristine SnS_2 nanoplates and (b) Au–SnS_2 nanohybrid.

© 2026 The Author(s). Published by the Royal Society of Chemistry

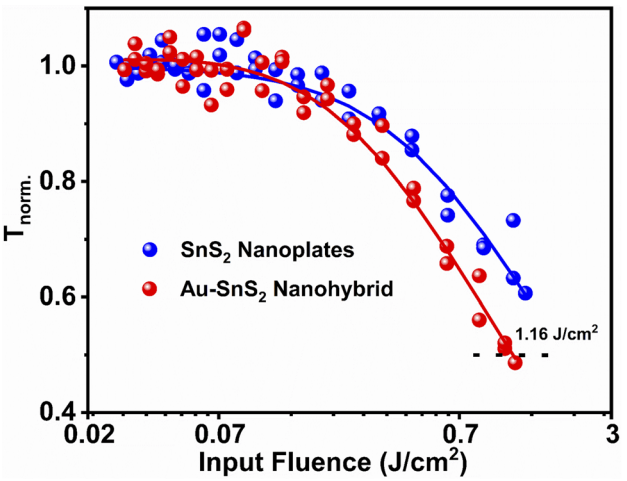


Fig. 7 Optical limiting plots of pure SnS_2 nanoplates and Au–SnS_2 nanohybrid.

and S_2 represent the ground state, first excited state and higher excited state, respectively. As the band gap energy of SnS_2 nanoplates is slightly lower than the incident photon energy, the laser pulse can enable efficient excitation of electrons from S_0 to S_1 (ground state absorption). Following this, if the electron in state S_1 absorbs an additional photon, it will be excited to the higher energy state S_2 leading to a phenomenon called excited state absorption as shown in Fig. 6(a). A reduction in the β_{eff} value from 50 cm GW^{-1} to 37 cm GW^{-1} was observed as the pulse energy increased from 10 μJ to 20 μJ. Similar intensity-dependent behaviour has been reported for SnS_2 nanosheets and other nonlinear optical nanomaterials under nanosecond excitation, where ESA was identified as the dominant nonlinear absorption mechanism.[16,42] However, the contribution of two-photon absorption cannot be completely ruled out. To further understand the origin of the observed RSA-like behaviour, the ground state absorption cross-sections (σ_g) and excited state absorption cross-sections (σ_e) of the SnS_2 nanoplates were calculated using the formulas, $\sigma_g = \frac{\alpha}{N_A C}$ and $\sigma_e = \frac{h\nu\beta_{eff}}{N_A C}$, respectively.[43,44] Here, $\alpha = 2.2$ cm^{-1} represents the linear absorption coefficient, N_A is the Avogadro's number, h is the Planck's constant, ν is the frequency of light and $C = 0.27$ μmol cm^{-3} represents the concentration of SnS_2 used for the Z-scan measurement at 10 μJ. The values of σ_g and σ_e were found to be 1.36×10^{-17} cm^2 and 8.47×10^{-17} cm^2, respectively. The significantly larger value of σ_e compared to σ_g further supports ESA as the dominant mechanism responsible for the observed RSA-like behaviour.[45]

As shown in Fig. 3(a), the wavelength of the laser photons lies well within the plasmonic absorption band of Au NPs used in the present study, which indicates that there is a high probability for resonant absorption. When the laser pulses are incident on Au–SnS_2 nanohybrid, strong electromagnetic fields will be generated around the Au NPs due to localized surface plasmon resonance effect as shown in Fig. 5. Interaction of this intense plasmonic field with the surrounding SnS_2 nanoplates enhances excitation of electrons from (i) S_0 to S_1 and (ii) S_1 to S_2 as schematically represented in Fig. 6(b). In addition, the Au NPs can also act as suppliers of hot-electrons. Hot-electron injection from metal nanoparticles to various MDC semiconductors such as MoS_2, WS_2 and WSe_2 has been reported in earlier studies.[46,47] According to the literature, SnS_2 exhibits lower work function (4.4–4.9 eV)[48,49] compared to Au (5.1 eV). Therefore, when Au NPs make intimate contact with the SnS_2 nanoplates in the nanohybrid, electrons from the conduction band of SnS_2 will flow to Au side till their Fermi levels are equal at equilibrium, leading to the band bending and Schottky barrier formation at the Au/SnS_2 interface. During laser light illumination, when plasmons in Au nanoparticle decay non-radiatively, the resulting high energetic electrons may overcome the energy barrier at the Au/SnS_2 interface and move to the excited state S_1 of SnS_2 as shown in Fig. 6(b). Rise in the electron population in the state S_1 due to the above-mentioned factors further enhance excited state absorption. Hence, the Au–SnS_2 nanohybrid exhibits superior RSA-like behaviour compared to the pristine SnS_2 nanoplates.

The enhanced nonlinear absorption exhibited by Au–SnS_2 nanohybrid is beneficial for optical limiting applications. The materials with strong optical limiting behavior, which transmit low intensity radiation and decrease the transmittance at higher intensities, are highly desirable for the development of laser safety devices that protect optical sensors and human from high power laser radiation. The performance of an optical limiting material is characterized by the onset value and limiting

Table 2 Comparison of nonlinear absorption coefficient and limiting threshold values of SnS_2 nanoplates and Au–SnS_2 nanohybrid obtained in the present study with the values reported for similar 2D materials and their nanohybrids measured at 532 nm wavelength

Material	Sample form	Peak intensity/(GW cm^{-2})	Pulse duration	β_{eff} (cm GW^{-1})	Limiting threshold (J cm^{-2})
SnS_2 nanoplates (present study)	Dispersion	0.27	7 ns	50	
WS_2 [28]	Dispersion	0.27	7 ns	47	
VS_2 nanosheets[39]	Dispersion	0.83	7 ns	27	4.2
TiS_2 nanosheets[5]	Dispersion	0.713	5 ns	80	
MoS_2 [50]	Dispersion		8 ns	62	
Au–SnS_2 nanohybrid (present study)	Dispersion	0.27	7 ns	85	1.16
Au-WS_2 nanohybrids[28]	Dispersion	0.27	7 ns	134	0.55
Ag-graphene oxide[51]	Dispersion	0.2	10 ns	45.4	6.4
Au NPs-rGO NS[52]	Dispersion	0.78	5 ns	66	0.6
Au@Ag Nw/MoS_2 [50]	Dispersion		8 ns	126.4	

© 2026 The Author(s). Published by the Royal Society of Chemistry

threshold. The onset value refers to the minimum input fluence at which the transmittance starts decreasing from its initial constant value. On other hand, the limiting threshold is defined as the input fluence at which the transmittance reduces to half of its initial value. To understand the optical limiting properties of the samples, variation of normalized transmittance with input fluence is carefully analyzed at 10 μJ pulse energy and presented in Fig. 7. In the case of bare SnS_2 nanoplates, though there is a significant optical limiting behavior, the transmittance has not reached the limiting threshold. On the other hand, due to the plasmon-enhanced light–matter interaction, Au–SnS_2 nanohybrid has shown strong optical limiting activity exhibiting onset value and limiting threshold of 0.07 J cm^{-2} and 1.16 J cm^{-2}, respectively. A comparative study presented in Table 2 indicates that the limiting threshold and onset values obtained in this work are significant compared to the values previously reported for similar 2D materials and their nanohybrids. Present study reveals that utilizing plasmonic effects of metal nanostructures is a powerful technique to improve the NLO properties of MDC nanostructures.

Conclusion

In summary, spherical Au NPs of diameter 20 nm and hexagonal SnS_2 nanoplates of average size 890 nm were synthesized using simple and cost-effective chemical methods. Their morphological, structural and optical properties were systematically investigated. The Au–SnS_2 nanohybrids were prepared by mixing pre-synthesized Au NPs and SnS_2 nanoplates. The NLO response of pristine nanostructures and the nanohybrid was recorded using Z-scan technique with a pulsed laser operating at 532 nm wavelength. Substantial enhancement in nonlinear absorption of SnS_2 nanoplates leading to improved optical limiting activity was observed after incorporating Au NPs. The superior optical limiting behavior exhibited by Au–SnS_2 nanohybrids is attributed to enhancement in excited state absorption due to the plasmonic effects of Au NPs. In addition, theoretical simulations were used to unveil the mechanism for enhancement of NLO activity in the nanohybrid. Present study demonstrates that the application potential of MDCs in the area of photonic devices can be improved by combining their inherent properties with the plasmonic effects of metal nanostructures.

Author contributions

Adarsh Raj K. P.: data curation (equal); formal analysis (lead); investigation (lead); writing – original draft (lead), visualization (lead). Hasana Jahan Elamkulavan: data curation (equal); formal analysis (supporting); investigation (supporting); writing – review and editing (supporting). Anoop C Sathyadevan Nair: data curation (supporting); investigation (supporting); formal analysis (supporting). Abhinand Ramachandran: data curation (supporting); visualization (supporting). Abhijith Thazhathenair: data curation (supporting); formal analysis (supporting); writing – review and editing (equal). Chandrasekharan Keloth: conceptualization (supporting); supervision (supporting); writing – review and editing (equal). Vari Sivaji Reddy: funding acquisition (lead); project administration (lead); conceptualization (lead); formal analysis (equal); supervision (lead); writing – review and editing (equal). All authors have given approval to the final version of the manuscript.

Conflicts of interest

The authors declare no conflict of interest.

Data availability

The data supporting this study, are available within the article and its supplementary information (SI). Supplementary information: size distribution histogram of SnS_2 nanoplates, FE-SEM image of SnS_2 nanoplates, EDS spectra and EDS colour mapping images of SnS_2 nanoplates, XRD pattern of SnS_2 nanoplates, Size distribution histogram of Au nanoparticles, HR-TEM image of Au–SnS_2 nanohybrid, Tauc plot of SnS_2 nanoplates and absorption spectra of Au–SnS_2 nanohybrid. See DOI: https://doi.org/10.1039/d6ra05188j.

Acknowledgements

The authors thank the Science and Engineering Research Board (SERB) for partially supporting this work under Core Research Grant (CRG) (Project File No. CRG/2021/001795). The XRD facility at Dept. of Physics, NIT Calicut (DST-FIST) is gratefully acknowledged. The authors acknowledge Dr Nithyanandan Kanagaraj and Ms. Bharathy Jacob, Department of Physics, IIT Hyderabad for FDTD simulations. The authors also acknowledge Dr Parameswaran P for valuable suggestions. AT acknowledges PSG Management Trustee and PSG Institute of Advanced Studies for providing the financial support through the Faculty Seed Research Grant.

References

1 S. Rahman and Y. Lu, *Nanoscale Horiz.*, 2022, **7**, 849–872.
2 Y. Meng, H. Zhong, Z. Xu, T. He, J. S. Kim, S. Han, S. Kim, S. Park, Y. Shen, M. Gong, Q. Xiao and S.-H. Bae, *Nanoscale Horiz.*, 2023, **8**, 1345–1365.
3 V. Shanmugam, R. A. Mensah, K. Babu, S. Gawusu, A. Chanda, Y. Tu, R. E. Neisiany, M. Försth, G. Sas and O. Das, *Part. Part. Syst. Charact.*, 2022, **39**, 2200031.
4 N. R. Glavin, R. Rao, V. Varshney, E. Bianco, A. Apte, A. Roy, E. Ringe and P. M. Ajayan, *Adv. Mater.*, 2020, **32**, 1904302.
5 S. J. Varma, J. Kumar, Y. Liu, K. Layne, J. Wu, C. Liang, Y. Nakanishi, A. Aliyan, W. Yang, P. M. Ajayan and J. Thomas, *Adv. Opt. Mater.*, 2017, **5**, 1700713.
6 M. Stavrou, N. Chazapis, E. Nikoli, R. Arenal, N. Tagmatarchis and S. Couris, *ACS Appl. Nano Mater.*, 2022, **5**, 16674–16686.
7 N. A. A. Kadir, E. I. Ismail, A. A. Latiff, H. Ahmad, H. Arof and S. W. Harun, *Chin. Phys. Lett.*, 2017, **34**, 014202.
8 X. Wen, Z. Gong and D. Li, *InfoMat*, 2019, **1**, 317–337.

© 2026 The Author(s). Published by the Royal Society of Chemistry

9 K. Ko, M. Jang, J. Kwon and J. Suh, *J. Appl. Phys.*, 2024, **135**, 100901.
10 Y. Rui, T. Li, B. Li, Y. Wang and P. Müller-Buschbaum, *J. Mater. Chem. C*, 2022, **10**, 12392–12401.
11 L. Xu, P. Zhang, H. Jiang, X. Wang, F. Chen, Z. Hu, Y. Gong, L. Shang, J. Zhang, K. Jiang and J. Chu, *Small*, 2019, **15**, 1904116.
12 F. Huang, J. Chen, C. Du, Q. Zhang, Y. Ding and W. Huang, *ACS Appl. Electron. Mater.*, 2022, **4**, 5333–5339.
13 X. Guo, F. Zhang, Y. Zhang and J. Hu, *J. Mater. Chem. A*, 2023, **11**, 7331–7343.
14 L. Shooshtari, N. Rafiefard, M. Barzegar, S. Fardindoost, A. Irajizad and R. Mohammadpour, *ACS Appl. Nano Mater.*, 2022, **5**, 17123–17132.
15 D. Zhang, G. Lu, Y. Qiu, S. Qin, H. Wang, J. Jiang, W. Zhou, P. Zhang, H. An and X. Li, *Ann. Phys.c*, 2022, **534**, 2200055.
16 J.-J. Wu, Y.-R. Tao, X.-C. Wu and Y. Chun, *J. Alloys Compd.*, 2017, **713**, 38–45.
17 Z. Wei, Y. Fang, H. Li, Z. Guan, N. Shan, F. Liu, Y. Zhao, L. Fu, Z. Huang, M. G. Humphrey and C. Zhang, *J. Mater. Chem. C*, 2023, **11**, 5190–5198.
18 M. Diao, H. Li, Y. Sun, Y. Liang, Z. Yu, D. W. Boukhvalov, Z. Huang and C. Zhang, *ACS Appl. Mater. Interfaces*, 2021, **13**, 4211–4219.
19 Y. Ke, D. W. Boukhvalov, M. G. Humphrey, C. Zhang and Z. Huang, *Adv. Opt. Mater.*, 2025, **13**, e02300.
20 H. Li, M. Diao, D. W. Boukhvalov, Y. Ke, M. G. Humphrey, C. Zhang and Z. Huang, *Adv. Funct. Mater.*, 2024, **34**, 2400077.
21 T. Abhijith, R. Suthar and S. Karak, *ACS Appl. Nano Mater.*, 2023, **6**, 11737–11746.
22 V. Selamneni, A. Mukherjee, H. Raghavan, P. T. Gomathi, C. S. R. Kolli, S. Pal, A. Hazra and P. Sahatiya, *ACS Appl. Nano Mater.*, 2022, **5**, 11381–11390.
23 Y.-M. Lin, C.-M. Wu, Y.-H. Lin, J.-H. Chang, L.-Y. Liang, V. K. S. Hsiao and C.-C. Chu, *ACS Omega*, 2024, **9**, 38778–38787.
24 K. Wang, D.-W. Sun, H. Pu, Q. Wei and L. Huang, *ACS Appl. Mater. Interfaces*, 2019, **11**, 29177–29186.
25 L. Zhou, Q. Huang and Y. Xia, *Chem. Rev.*, 2024, **124**, 8597–8619.
26 A. Srivastava, D. P. Samajdar and D. Sharma, *Sol. Energy*, 2018, **173**, 905–919.
27 M. N. Vengoli, P. Nancy, R. Antoine and N. Kalarikkal, *ACS Appl. Opt. Mater.*, 2025, **3**, 1921–1933.
28 A. T, S. Edappadikkunnummal, R. Suthar, S. Thomas and S. Karak, *ACS Appl. Nano Mater.*, 2023, **6**, 2327–2335.
29 J. Hu, J. Zhang, X. Liu, H. Zhang, X.-X. Xue and Y. Zhang, *Appl. Surf. Sci.*, 2023, **623**, 157093.
30 S. Das, T. Dey, D. Mandal, S. K. Ray, P. Banerji, A. Chandra and R. Basori, *J. Appl. Phys.*, 2025, **137**, 233103.
31 R. Fu, L. Li, X. Li, B. Li, C. Shao, Z. Liu and A. Shen, *Mater. Chem. Phys.*, 2021, **267**, 124702.
32 R. Lucena, F. Fresno and J. C. Conesa, *Appl. Catal., A*, 2012, **415–416**, 111–117.
33 G. Frens, *Nat. Phys. Sci.*, 1973, **241**, 20–22.
34 J. Xia, D. Zhu, L. Wang, B. Huang, X. Huang and X. Meng, *Adv. Funct. Mater.*, 2015, **25**, 4255–4261.
35 A. B. Tambe, N. S. Jawale, S. S. Arbuj, G. G. Umarji, R. Kadari, S. Kulkarni and B. B. Kale, *Langmuir*, 2025, **41**, 15892–15908.
36 S. Edappadikkunnummal, S. N. Nherakkayyil, V. Kuttippurath, D. M. Chalil, N. R. Desai and C. Keloth, *J. Phys. Chem. C*, 2017, **121**, 26976–26986.
37 A. Mohanty and K. Kamali, *ACS Appl. Nano Mater.*, 2024, **7**, 3326–3338.
38 Nikhil, R. Shyam, R. Baranwal, S. Verma and S. Gangolu, *ACS Appl. Electron. Mater.*, 2026, **8**, 3843–3856.
39 A. Joseph, H. J. Elamkulavan, C. Keloth and P. M. Aneesh, *ACS Appl. Opt. Mater.*, 2023, **1**, 1688–1696.
40 G. Wang, A. A. Baker-Murray and W. J. Blau, *Laser Photon. Rev.*, 2019, **13**, 1800282.
41 G. A. Ermolaev, D. I. Yakubovsky, M. A. El-Sayed, M. K. Tatmyshevskiy, A. B. Mazitov, A. A. Popkova, I. M. Antropov, V. O. Bessonov, A. S. Slavich, G. I. Tselikov, I. A. Kruglov, S. M. Novikov, A. A. Vyshnevyy, A. A. Fedyanin, A. V. Arsenin and V. S. Volkov, *Nanomaterials*, 2021, **12**, 141.
42 S. Edappadikkunnummal, S. N. Nherakkayyil, V. Kuttippurath, D. M. Chalil, N. R. Desai and C. Keloth, *J. Phys. Chem. C*, 2017, **121**, 26976–26986.
43 P. P. Kiran, D. R. Reddy, A. K. Dharmadhikari, B. G. Maiya, G. R. Kumar and D. N. Rao, *Chem. Phys. Lett.*, 2006, **418**, 442–447.
44 J. Jia, X. Wu, Y. Fang, J. Yang, Y. Han, J. Xiao, X. Zhang, Y. Wang and Y. Song, *J. Phys. Chem. C*, 2020, **124**, 4701–4708.
45 N. P. Purayil, A. K. Satheesan, S. Edappadikkunnummal and C. Keloth, *J. Phys. Chem. C*, 2023, **127**, 1244–1250.
46 C. Xu, H. W. Yong, J. He, R. Long, A. R. Cadore, I. Paradisanos, A. K. Ott, G. Soavi, S. Tongay, G. Cerullo, A. C. Ferrari, O. V. Prezhdo and Z.-H. Loh, *ACS Nano*, 2021, **15**, 819–828.
47 J. Tang, Y. Li, S. Ye, P. Jiang, Z. Xue, X. Li, X. Lyu, Q. Liu, S. Chu, H. Yang, C. Wu, X. Hu, Y. Gao, S. Wang, Q. Sun, G. Lu and Q. Gong, *Nano Lett.*, 2024, **24**, 2931–2938.
48 Q. Sun, Y. Li, J. Hao, S. Zheng, T. Zhang, T. Wang, R. Wu, H. Fang and Y. Wang, *ACS Appl. Mater. Interfaces*, 2021, **13**, 54152–54161.
49 G. Ham, S. Shin, J. Park, H. Choi, J. Kim, Y.-A. Lee, H. Seo and H. Jeon, *ACS Appl. Mater. Interfaces*, 2013, **5**, 8889–8896.
50 M. N. Vengoli, P. Nancy, R. Antoine and N. Kalarikkal, *ACS Appl. Opt. Mater.*, 2025, **3**, 1921–1933.
51 S. Biswas, A. K. Kole, C. S. Tiwary and P. Kumbhakar, *RSC Adv.*, 2016, **6**, 10319–10325.
52 R. K. Yadav, J. Aneesh, R. Sharma, P. Abhiramnath, T. K. Maji, G. J. Omar, A. K. Mishra, D. Karmakar and K. V. Adarsh, *Phys. Rev. Appl.*, 2018, **9**, 044043.

© 2026 The Author(s). Published by the Royal Society of Chemistry